Earth's Future

RESEARCH ARTICLE
10.1029/2020EF001824

Key Points:

- What is now a 20-years rainfall will become a 7-year rainfall for ~75% of gridpoints over the US
- Rainfall extreme intensification is mostly expressed with increases in tail heaviness
- Future rainfall extremes are more uniformly distributed throughout the year and have shorter duration

Supporting Information:

- Supporting Information S1

Correspondence to:
Y. Moustakis,
i.moustakis18@imperial.ac.uk

Citation:
Moustakis, Y., Papalexiou, S. M., Onof, C. J., & Paschalis, A. (2021). Seasonality, intensity, and duration of rainfall extremes change in a warmer climate. *Earth's Future*, *9*, e2020EF001824. https://doi.org/10.1029/2020EF001824

Received 24 SEP 2020
Accepted 16 FEB 2021

Seasonality, Intensity, and Duration of Rainfall Extremes Change in a Warmer Climate

Yiannis Moustakis[1], Simon Michael Papalexiou[2], Christian J Onof[1], and Athanasios Paschalis[1]

[1]Department of Civil and Environmental Engineering, Imperial College London, London, UK, [2]Department of Civil, Geological and Environmental Engineering, University of Saskatchewan, Saskatoon, Canada

Abstract Precipitation extremes are expected to intensify under climate change with consequent impacts in flooding and ecosystem functioning. Here we use station data and high-resolution simulations from the WRF convection permitting climate model (~4 km, 1 h) over the US to assess future changes in hourly precipitation extremes. It is demonstrated that hourly precipitation extremes and storm depths are expected to intensify under climate change and what is now a 20-year rainfall will become a 7-year rainfall on average for ~ 75% of gridpoints over the US. This intensification is mostly expressed as an increase in rainfall tail heaviness. Statistically significant changes in the seasonality and duration of rainfall extremes are also exhibited over ~ 95% of the domain. Our results suggest more non-linear future precipitation extremes with shorter spell duration that are distributed more uniformly throughout the year.

Plain Language Summary Rainfall extremes are intensifying under climate change and are expected to have an impact on ecosystem functioning and catchment flood responses. Here, we use state-of-the-art high-resolution convection permitting model simulations and station data to examine future changes in the statistical properties of rainfall extremes in a warmer climate. Our results reveal a severe intensification of rainfall extremes throughout the US in a warmer climate, with a less pronounced seasonal signal and decreased spell duration.

1. Introduction

Increasing trends and changes in the frequency of Precipitation Extremes (PEx) have already been observed (Guerreiro et al., 2018; Hoerling et al., 2016; Markonis et al., 2019; Papalexiou & Montanari, 2019; Westra et al., 2014) and intensification is expected to be more prominent in a future warmer climate (Fischer & Knutti, 2014; Fischer et al., 2013, 2014; Pendergrass & Hartmann, 2014; Pfahl et al., 2017). A wide scientific consensus is being built with increasing confidence upon this robust agreement between theory, models and observational data (Fischer & Knutti, 2016). In their effort to become more resilient to the upcoming natural disasters (Cutter et al., 2008), communities need to be aware of the expected PEx intensification and its associated risks, and hence, understanding the mechanisms driving this change is of crucial importance. However, predictions regarding PEx at the hourly scale, which is more relevant for hydrological design (Paschalis et al., 2014) and ecosystem functioning (Paschalis et al., 2015, 2020), remain challenging and have not been extensively studied (Westra et al., 2014).

According to the Clausius-Clapeyron (CC) relation warmer air can hold more moisture at a rate of ~7%/K and it has been suggested that PEx should be increasing with rising temperature roughly at the same rate (Lenderink & Van Meijgaard, 2008). Indeed, Moustakis et al. (2020) recently demonstrated in a global study that this relationship holds over most parts of the mid- and high-latitudes for hourly PEx, while deviations were found over the (sub-) tropics. On the contrary, changes in the body of rainfall distributions are constrained by the atmospheric energy budget at a lower rate of ~2%/K (Held & Soden, 2006). However, the complexity of precipitating systems and the interplay between thermodynamic and dynamic factors enhancing or diminishing precipitation formation shed doubt over approaches based on thermodynamic scaling alone (Moustakis et al., 2020; O'Gorman, 2015; Pfahl et al., 2017). Changes in temperature lapse rate, upward wind velocity and large-scale moisture convergence, accompanied by shifts in the Intertropical Convergence Zone's strength, width and location are expected to jointly shape the future state of precipitation extremes globally (Byrne et al., 2018; O'Gorman, 2015; O'Gorman & Schneider, 2009). As we progress

from regional to local scales, uncertainty due to internal variability remains irreducible (Fischer et al., 2013; Fatichi, Ivanov, et al., 2016) and topographical features and the area-specific weather patterns will also determine the magnitude and direction of change (Moustakis et al., 2020), thereby increasing the difficulty of making predictions.

Climate models operating at coarse spatial scales do not explicitly resolve processes occurring at the local scale and convection is instead parameterized (Prein et al., 2015). Such models are incapable of properly simulating PEx, especially over regions experiencing deep convection and orographic enhancement (Prein et al., 2015). Recently, given the increasingly available computational capabilities, convection-permitting models (CPM) operating at fine spatial resolutions (kilometer scale) have been used yielding promising results (Ban et al., 2018; Kendon et al., 2017; Prein et al., 2015). Such model outputs allow for a more detailed investigation of storm producing environments and changes in rainfall distributions for the first time.

Continental-wide applications have recently been performed (Berthou et al., 2018; Chan et al., 2020; Knist et al., 2020; Liu et al., 2017; Stratton et al., 2018), with the longest being two 13-year simulations of present (CTL) and future (PGW) climate over the US with the Weather Research and Forecasting (WRF) CPM (Liu et al., 2017). Studies based on these simulations have revealed the expected changes in the distribution of rainfall (Dai et al., 2017) and the intensity-duration-frequency curves (Cannon & Innocenti, 2019), the formation, organization and propagation of Mesoscale Convective Systems (MSC) (Prein, Liu, Ikeda, Bullock, et al., 2017; Prein, Rasmussen, et al., 2017), the diurnal cycle of PEx (Scaff et al., 2019) and the features of convective environments (Rasmussen et al., 2017).

However, a detailed investigation of changes in rainfall tails has not been made yet. The term *tail* refers to the upper parts of the complementary cumulative distribution function (i.e. survival function) and expresses the likelihood of PEx occurrence. Investigating the statistical properties of rainfall tails and their future changes is crucial for the scientific community in order to properly assess future flood risk. However, focus should not be limited only to PEx changes, but changes in the total Storm Depth Extremes (SDEx), which are more directly related to flood volumes should be studied as well.

In this study we focus on: (1) the spatial pattern of the statistical properties of rainfall tails across the US, (2) future changes in PEx/SDEx, (3) their seasonality, (4) SDEx durations, and (5) conceptualizing PEx intensification in relation to different storm producing environments affecting a region. We reveal increases in tail heaviness over most of the domain both in hourly precipitation and storm depths. Increases in heaviness lead to larger and more frequent extremes and indicate an intensification beyond expectations based on basic thermodynamic approaches. Significant changes in seasonality and event duration are also evident. Such changes could jointly affect the coupled water-carbon dynamics in ecosystems and significantly alter catchment flood responses, thus further increasing future flood risk.

2. Data

The hourly precipitation NOAA -ISD and -HPD datasets are used in this study. It is considered that at least 3,000 values of non-zero hourly rainfall are necessary in order to evaluate the tails of rainfall with confidence (Papalexiou, AghaKouchak, & Foufoula-Georgiou, 2018), and only station records exceeding this threshold have been used. All values flagged as possibly spurious have been treated as missing. The final pool of station data consists of 3,119 stations, located in the Contiguous United States (Figure S1). Spatial interpolation of station data is performed with an inverse distance weight function.

The climate simulations used in this study are an output of the Weather Research and Forecasting (WRF) model, which is is a convection permitting climate model (CPM) operating at a 4 km resolution. The present WRF simulation (CTL-WRF) (Liu et al., 2017) used in this study is a retrospective simulation of the present climate spanning from October 2000 to September 2013 that is driven by ECMWF's 6-h ERA-Interim reanalysis data. Given that WRF model biases exhibited at the local scale may affect and contaminate the larger-scale dynamics that are forcing the simulation, spectral nudging has also been applied, and hence, larger-scale dynamics remain relatively unchanged (Liu et al., 2017).

The future WRF simulation (PGW-WRF) (Liu et al., 2017) is a simulation of the future climate under the RCP8.5 scenario, realized with a pseudo global warming (PGW) approach. Under the PGW experiment,

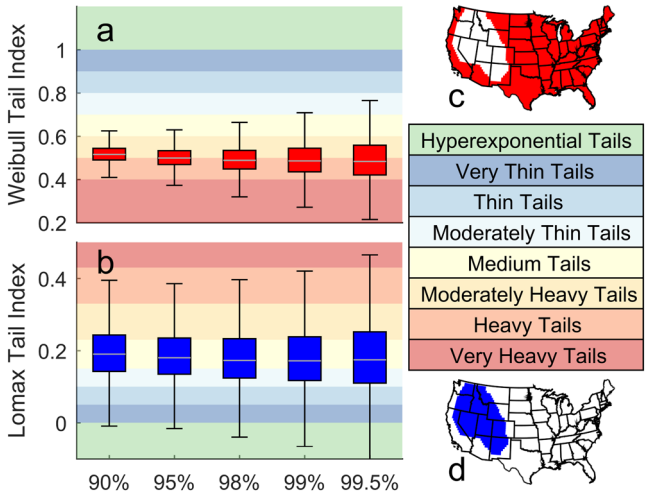

Figure 1. Assessment of the robustness of the distributions used: Boxplots of the (a) Weibull and (b) Lomax shape parameter (tail index) for tails defined with different quantiles of non-zero hourly rainfall. Different colors indicate different levels of heaviness as indicated by the colormap. (c) Red and (d) blue color indicate gridpoints where the Weibull and Lomax are used respectively.

ERA-Interm's boundary conditions are perturbed by the 95-year multi-model (19 GCMs) ensemble-mean climate change signal corresponding to the periods 1976–2005 and 2071–2100 (Liu et al., 2017).

A 2-D median filtering within a 10 × 10 moving window is applied on all maps showing WRF results to reduce noise. Only values exceeding 0.1 mm/h are considered as non-zero values and only gridpoints with at least 3,000 non-zero values are examined. We make use of the Bukovsky (2011) regionalization, which classifies eco-regions of similar regional climatological characteristics to aid in our analysis.

3. Methods

3.1. Statistics of Rainfall Extremes

The tail of the distribution of non-zero hourly rainfall extremes (PEx) is defined as the part of the distribution exceeding a certain threshold. In order to estimate the tails of SDEx statistically independent rainfall events are defined as those separated by a 2-h dry interval (supporting information's Methods). Since extreme flooding does not necessarily occur when the rarest PEx occur, but is rather conditioned on antecedent soil moisture (Ali et al., 2019; Sharma et al., 2018), we have chosen a tail definition that is not limited and sensitive only to the rarest PEx. Hence, we use the 0.95^{th} quantile throughout the study. Given the relatively small WRF sample size and the absence of multiple ensemble members, using higher quantile levels would make our analysis subject to higher uncertainty. However, the 0.90^{th}, 0.98^{th}, 0.99^{th}, and 0.995^{th} quantiles have also been examined, yielding similar results. Tail analyses are also performed for the cold (October-March) and warm (April-September) periods separately (supporting information's Methods).

The Lomax (Pareto type II), which is a power-type distribution and the Weibull, which follows an exponential form are used to describe tails, following Equations 1 and 2 respectively:

$$F_L(x) = \left(1 + \gamma \frac{x}{\beta}\right)^{-\frac{1}{\gamma}} \tag{1}$$

$$F_W(x) = \exp\left(-\left(\frac{x}{\beta}\right)^{\gamma}\right) \tag{2}$$

where $\beta > 0$ is the scale and γ (Weibull $\gamma > 0$) is the shape parameter (tail index). These distributions are widely popular across different scientific fields and have been found to perform well in describing hourly PEx (Papalexiou, AghaKouchak, & Foufoula-Georgiou, 2018) and jointly cover a wide range of tail types including power, exponential, stretched-exponential and hyper-exponential. Tails are fitted by minimizing the probability ratio mean square error (PRMSE) as in Papalexiou, AghaKouchak, and Foufoula-Georgiou (2018), thus making the fit insensitive to possible outliers, while equally weighting all tail values.

The tail index determines the "heaviness" of the tail (i.e. the rapidity with which the survival function approaches zero). The less rapidly a tail's survival function approaches zero, the heavier the tail is considered and hence extremes increase and become more frequent. Based on the tail index, we qualitatively define tails as very heavy, heavy, moderately heavy, medium, moderately thin, thin, very thin and hyperexponential (tails whose survival function approaches zero more rapidly than the exponential distribution) (Figure 1). According to the formulation of the Lomax (Weibull) distribution used here, higher (lower) tail indices indicate heavier tails.

Even though the scale parameter is mostly linked with rainfall amounts it remains a parameter of a mathematical formulation and does not have a straightforward physical meaning. Decreases in the scale parameter can occur due to large increases in heaviness even in cases where an intensification is evident (Figure S2) and slight decreases should not be misinterpreted as a sign of de-intensification. It is the joint change of both scale and shape parameters that determines the direction and magnitude of intensification.

In order to determine which distribution is more appropriate for describing rainfall tails over the domain we first fitted both the Weibull and Lomax distributions over all gridpoints based on the 0.90^{th}, 0.95^{th}, 0.98^{th}, 0.99^{th}, and 0.995^{th} quantiles. Theoretically, if a tail is properly described by a shape-scale parameter pair, then this pair should roughly hold for all quantiles used for defining the tail. As a result, the distribution that yields estimations that are more consistent throughout all quantiles can be considered as a better fit (Figures S3 and S4). The same results are obtained if decision is made based on PRMSE values (Figure S5). Negative tail index values for the Lomax distribution imply that an upper threshold in the rainfall tail exists. Even though this could have a physical basis, we refrain from strictly defining an upper PEx bound and over such regions (i.e. the Pacific coast) the Weibull was instead chosen, which also performs well (Figure S3).

3.2. Seasonality of Rainfall Extremes

The seasonality of rainfall extremes is defined here as the non-uniformity (i.e. distance of true distribution from the uniform distribution) of the distribution of monthly occurrences in the tail and indicates the tendency of extreme rainfall events to cluster within a specific period of time during the year. Non-uniformity is expressed as the Relative Entropy (RE) (Kullback-Leibler distance) (Cover & Joy, 2005; X. Feng et al., 2013), following Equation 3:

$$\mathrm{RE} = \sum_{m=1}^{12} p_m \log_2(p_m \,/\, q_m), \tag{3}$$

where, given the total number of tail values L and the number of tail values n_m having occurred at each given month m, the probability of occurrence per month is $p_m = n_m/L$, while q_m is the probability under the uniform distribution (i.e. 1/12 for each month). Seasonality values are then normalized. Higher values of RE indicate a stronger deviation from the uniform distribution. Of course, strong non-uniformity does not suggest that a distinct seasonal signal necessarily exists, however, this property holds throughout the domain (Figure S6), since PEx tails have a distinct seasonality and are mostly clustered within specific periods of the year. The seasonality index is further assessed under a Monte Carlo experiment and values < 0.08 (depending on sample size) may correspond to a uniform distribution (Figure S7).

Inference of statistical significance of our results has been performed with the methodology presented in supporting information's Methods.

4. Results

Our results show that the Lomax distribution (a power-type distribution also known as Pareto-II) is a better fit over the Great Basin and the Southern and Northern Rockies (from now on referred to as MtWest) where tails are mostly moderately thin to moderately heavy. The Weibull distribution (distribution of exponential form) performs better over the rest of the domain, with mostly (moderately) heavy tails (Figures 1 and S3–S5). The Lomax outperformed the Weibull distribution over the Pacific Northwest and Southwest (from now on referred to as Pacific coast) (Figures S3–S5), however negative tail indices were estimated and Weibull was chosen instead (see Methods). As expected the variability increases as higher quantile levels are used to define the tail due to decreasing sample sizes (Figures 1, S3 and S4) and uncertainty increases.

The basic features of the spatial pattern of shape parameters (tail indices) γ, based on 3,119 stations (Figure 2a) are in agreement with Papalexiou, AghaKouchak, and Foufoula-Georgiou (2018), who, however used the 0.995^{th} quantile and, hence differences are expected. Over the Pacific (very) thin tails appear, moderately heavy tails are prominent over MtWest and tails are heavy over the Southwest (Tables S1 and S2). Heavy tails are evident over the Northern Plains and the northernmost parts of the Prairie and the Great Lakes. Over parts of the Southeast and the Deep South (from now on referred to as South), a consistent

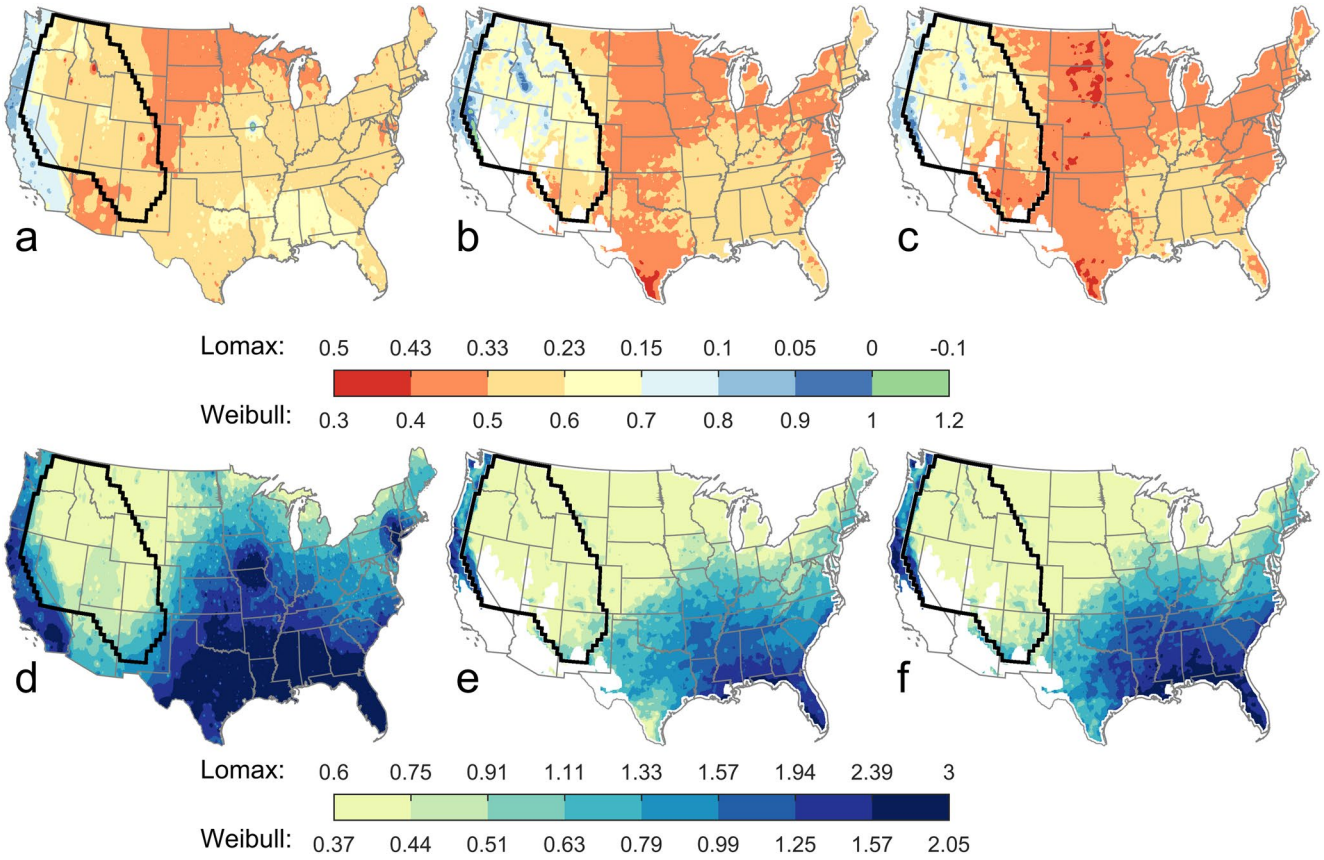

Figure 2. PEx tails spatial pattern: Maps of tail indices across the US based on (a) Station data, (b) CTL-WRF and (c) PGW-WRF simulations. The color scale corresponds to the qualitative classification of tail heaviness presented in Figure 1. Maps of the scale parameters across the US based on (d) Station data, (e) CTL-WRF, and (f) PGW-WRF simulations. The thick black line forms the outline of the region where the Lomax is used (Figure 1). PEx, Precipitation Extremes; PGW, Pseudo Global Warming; WRF, Weather Research and Forecasting model.

band of moderate tails is exhibited, while, over the rest of the domain moderately heavy tails are common. High values of the scale parameter β occur over the South, gradually decreasing toward the northwest and reaching the lowest values over MtWest and Northern Plains (Figure 2d). The scale parameter is increased over the Pacific coast.

The CTL-WRF simulation is able to represent the observed patterns, albeit with some biases (Figures 2b and 2e). Compared to station data CTL-WRF shows an east-west bias in estimating heaviness and a consistent underestimation of scale parameters throughout the domain. In particular, CTL-WRF exhibits thinner tails over MtWest and the Pacific coast, and heavier tails over the rest of the domain (Tables S1 and S2). Similar results are obtained when the Weibull and Lomax distributions are examined separately (Figures S8 and S9).

The PGW-WRF simulation yields a pattern with heavier tails and larger scale parameters than CTL-WRF, with changes being statistically significant throughout the domain (Figures 2c, 2f, and S10). Heaviness increases over MtWest, the Pacific coast, the Plains, the Prairie and the North Atlantic (Figures 3a and 3d). Over the South, the MidAtlantic and the Great Lakes increases in heaviness are less pronounced and more scattered. This image is roughly mirrored, with strong increases in scale parameter over the South and Mid-Atlantic (Figure 2f), decreases over the Northern and Central Plains, and moderate increases over MtWest and the Pacific coast. Intensification is also evident when spatially aggregated relative changes over high rainfall quantiles are examined (Figure S11).

During the cold period (Figures 3b and 3e), heaviness increases over most parts of the domain, but more strongly over the Pacific coast and the Mid- and North-Atlantic (from now on referred to as East coast). A

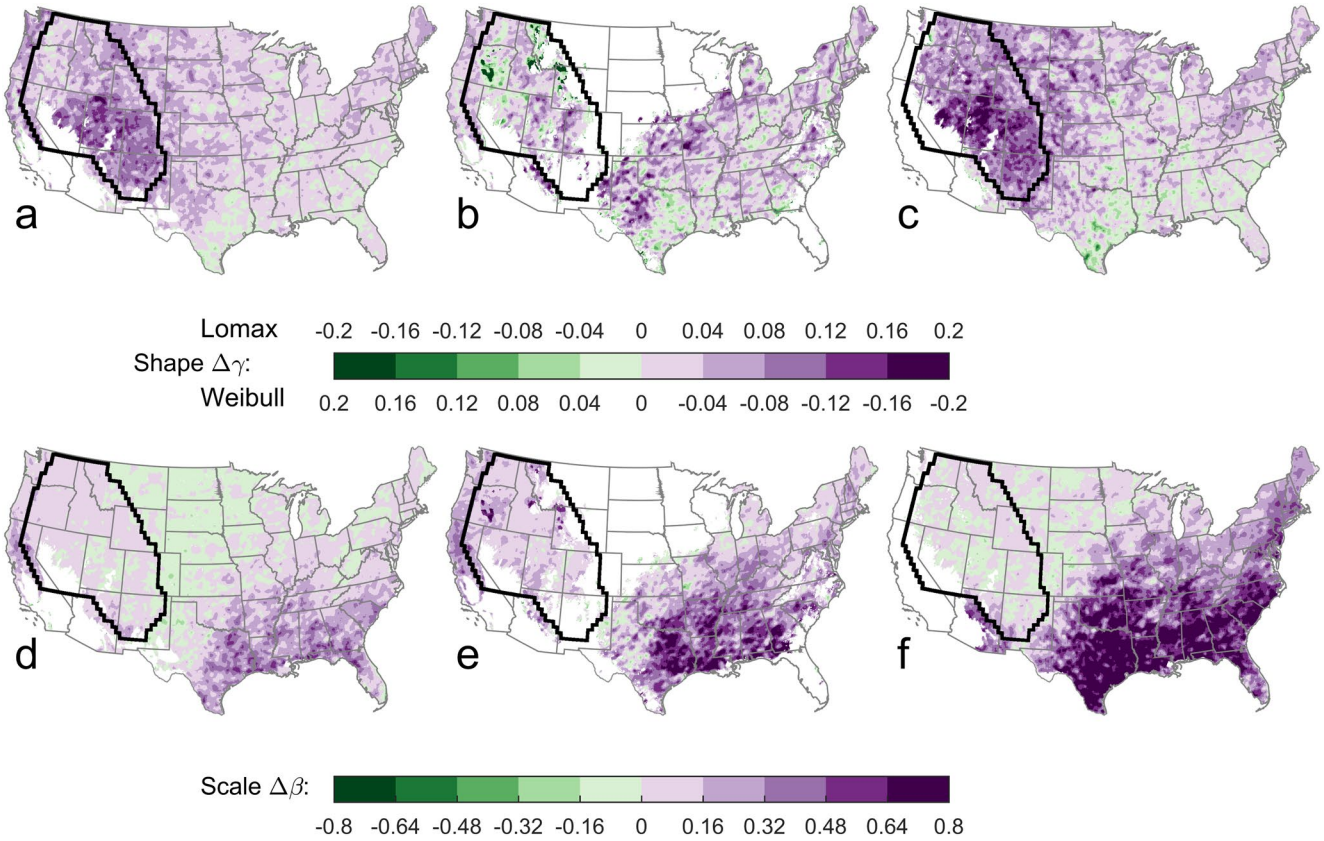

Figure 3. Future changes in PEx tails: Maps of differences in PEx shape and scale parameters between PGW-WRF and CTL-WRF simulations estimated based on the (a and d) full record, (b and e) cold months (October-March) and (c and f) warm months (April-September). Colormaps are adjusted so that purple color indicates intensification. The thick black line forms the outline of the region where the Lomax is used. Only gridpoints with statistically significant changes are shown. PEx, Precipitation Extremes; PGW, Pseudo Global Warming; WRF, Weather Research and Forecasting model.

more coherent spatial pattern of increases in scale parameters is exhibited over the domain, with greater increases over the South and the Pacific coast. During the warm period (Figures 3c and 3f), the changes are roughly similar to the changes obtained when the full record is used (Figures 3a and 3d). However, heaviness increases more notably over MtWest and the Plains. The scale parameter is severely increased over the South, the Southern Plains, the East Coast, Appalachia and the Prairie. Similar changes in distribution parameters are obtained when the Weibull and Lomax distributions are separately examined (Figures S12 and S13).

The analysis has also been performed for the tails of SDEx (Figure 4, Tables S3 and S4). The Lomax distribution fits better to SDEx tails and is, hence preferred (Figure S14). According to station data SDEx tails are moderately heavy and medium throughout most of the domain (Figure 4a) and a pattern with distinct spatial features is not obtained. The Pacific coast, the Northern Plains, the East coast and the northern parts of MtWest yield generally heavier tails, although differences are not strong (i.e. all regions lie mostly within the range 0.2–0.3). The scale parameter (Figure 4d) varies similarly with PEx (Figure 2d), although with larger values, since total storm depths are considered.

The CTL-WRF simulation adequately captures the spatial SDEx tail pattern (Figures 4b and 4e). However, an overestimation of heaviness is evident over the Plains, the South, the Mezquital and Southern Rockies, and an underestimation over the Great Basin, the Great Lakes, and the North Atlantic. The scale parameter is most notably overestimated over the North Atlantic and the western parts of the Pacific Coast where precipitation gets orographically enhanced upon meeting the mountain ranges and underestimated over the Plains and the South.

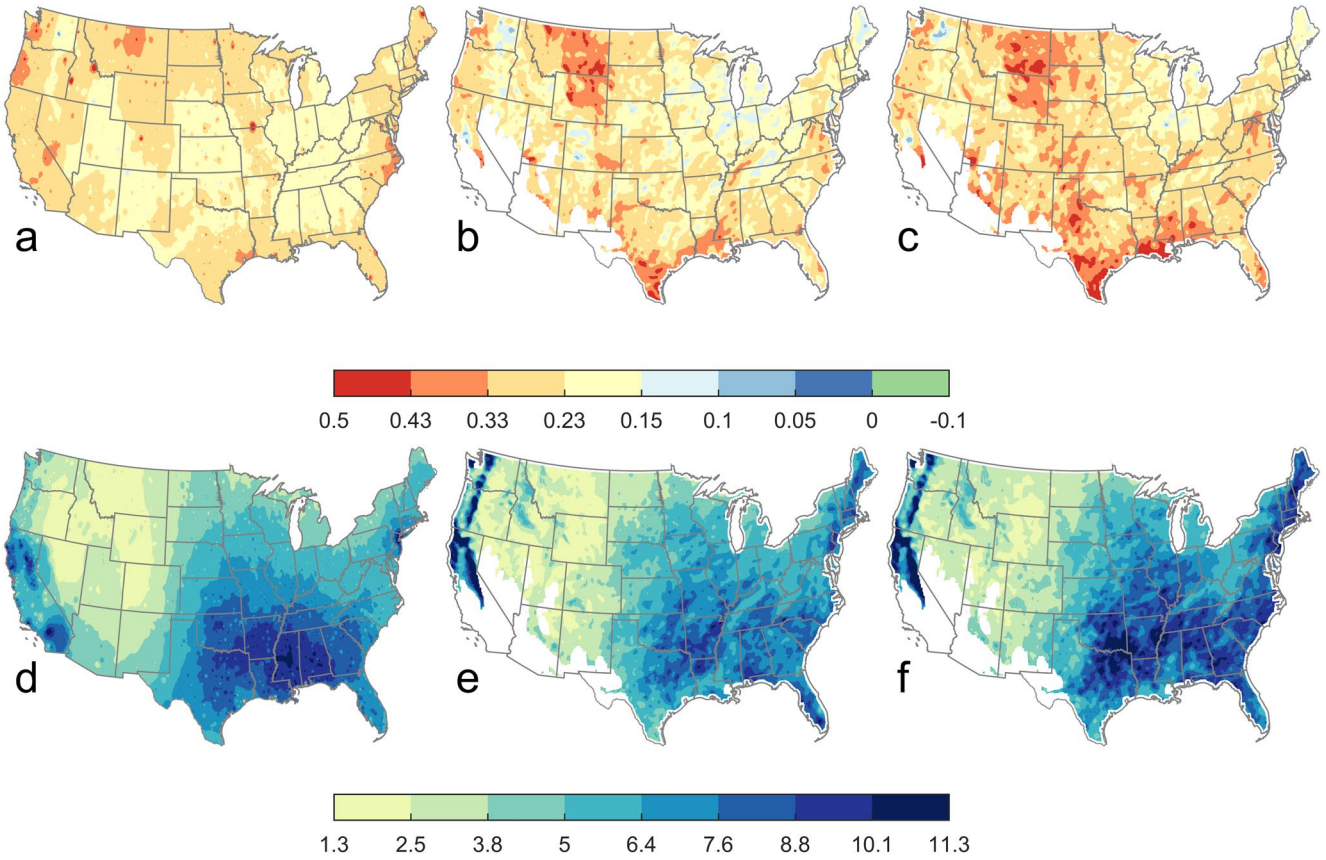

Figure 4. SDEx tails spatial pattern: same as Figure 2, but for SDEx. The parameters refer to the Lomax distribution which is a better fit for SDEx tails. SDEx, Storm Depth Extremes.

Under the PGW-WRF simulation, statistically significant changes are revealed. SDEx intensification is evident in terms of heaviness throughout the domain (Figure 4c), while scale parameter also increases (Figure 4f). Strong increases in heaviness seem to dominate the signal, which is however noisy (Figure 5a). Heaviness increases mostly over the Plains and the South and scale parameter over the East coast, the South and the Southern Plains (Figure 5b).

The CTL-WRF simulation can adequately capture the observed SDEx duration spatial pattern (Figures S15 and S16). Typically, Pacific Coast receives the longest SDEx (Tables S3 and S4). Large durations are also common over the East coast, followed by Appalachia, the South, the Great Lakes the Prairie and the Plains. Differences between station data and CTL-WRF are mostly induced by gauge resolution and can be alleviated by defining a different non-zero threshold (i.e. 0.01 inch, which is a typical lowest threshold in many gauges) (Figures S1, S15, and S16).

Statistically significant duration changes under PGW-WRF are exhibited over 96% of gridpoints, 69% of which are decreases. Decreases are more severe over the Pacific Coast and the North Atlantic and increases mostly over parts of the Prairie and the Great Lakes (Figure 6).

Observed PEx seasonality increases from the south toward the northwest (Figure 7a). Regions with low seasonality experience PEx throughout the year, while high seasonality suggests that PEx are clustered within certain periods during the year (Figure S6). Increased seasonality is evident over the Central and Northern Plains, the Prairie, the Mezquital and the Pacific Southwest. Seasonality is low over the South and the East coast (Tables S1 and S2). Seasonality decreases from the outermost toward the innermost parts of MtWest.

The CTL-WRF simulation adequately captures the observed seasonality pattern, with an underestimating bias over the Plains, the Prairie and Mezquital, while seasonality is overestimated over the Pacific coast and

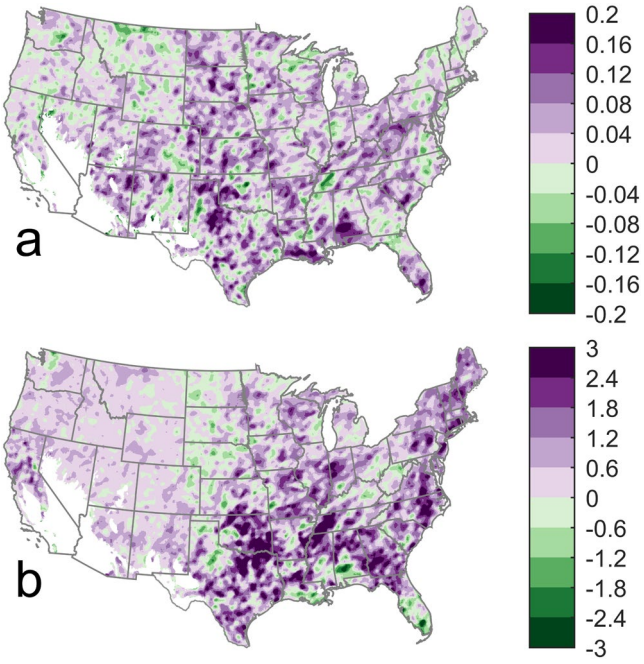

Figure 5. Future changes in SDEx tails: Maps of differences in the (a) shape and (b) scale parameters between the PGW-WRF and CTL-WRF simulations. Colormaps are adjusted so that purple color indicates intensification. The parameters refer to the Lomax distribution which is a better fit for SDEx tails. Only gridpoints with statistically significant changes are shown. PGW, Pseudo Global Warming; SDEx, Storm Depth Extremes; WRF, Weather Research and Forecasting model.

the Southeast (Figure 7b). Statistically significant changes in seasonality are revealed throughout the domain (Figures 7c and S7). It is evident that over the Central and Northern Plains, the Prairie, North Antlantic, the Appalachia and Southern and Northern Rockies seasonality decreases.

Roughly the same pattern is obtained when the seasonality of SDEx is examined (Figures 7d–7f). However, observed seasonality (Figure 7d) is weaker over the North Atlantic, the Appalachia and the Prairie, while it is stronger over the Pacific Coast (especially the southwestern parts) compared to PEx seasonality. CTL-WRF simulation (Figure 7e) captures the seasonality pattern adequately, with an underestimating bias over the Plains, and an overestimating bias over the Pacific Coast and over the northernmost MtWest. Statistically significant changes in SDEx seasonality (Figures 7f and S7) appear in 94% of gridpoints, 53% of which decrease. Most notably, seasonality decreases over parts of the Central and Northern Plains and the Northern Rockies and increases over parts of the Prairie, the South and Southern Plains.

An investigation of the rarest PEx (Figure 8, Table S1 and S3) reveals that what was a 20-year PEx (SDEx) estimated based on CTL-WRF, becomes more frequent and corresponds to smaller return periods in PGW-WRF for 75% (76%) of the domain gridpoints. The most extreme PEx intensification is observed over MtWest, the Pacific coast and the East Coast. PEx intensification is also strong over Appalachia, the Plains, the Great Lakes, and the Prairie. Intensification is also consistent throughout all eco-regions for SDEx, with Appalachia, Southern and Central Plains, the Prairie, Southern Rockies, the Great Lakes and the South facing the most severe intensification.

Aside from the statistical significance of changes revealed here, the probability that such changes lie within the uncertainty boundaries of CTL-WRF has also been assessed (Figures S7, S17, and S18). Changes in PEx/SDEx lie mostly outside the limits of CTL-WRF uncertainty boundaries throughout the domain. PEx seasonality decreases over the Plains, the Northern Rockies, the Prairie and the North Atlantic and SDEx duration decreases over the Pacific coast are also quite robust.

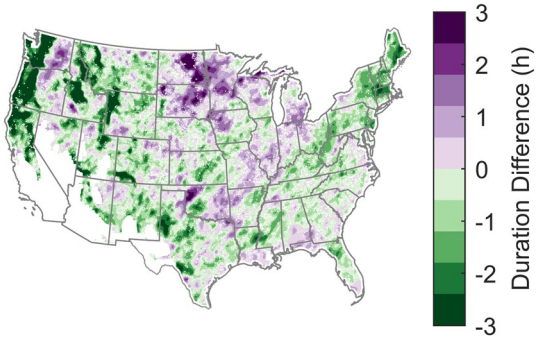

Figure 6. SDEx duration changes: Differences in mean SDEx duration (h) between the PGW-WRF and CTL-WRF. Purple color indicates an increase in duration. Only gridpoints with statistically significant changes in duration are shown. PGW, Pseudo Global Warming; SDEx, Storm Depth Extremes; WRF, Weather Research and Forecasting model.

5. Discussion

Here we demonstrate a consistent PEx/SDEx intensification throughout the domain, expressed with increases in the scale and shape parameters. Under a warmer climate PEx will be more uniformly spread throughout the year with more pronounced changes over the Plains, the Northern Rockies and the Prairie (Figures 7 and S7), while mixed responses are expected regarding SDEx seasonality. SDEx duration also changes, with decreases over the Pacific coast being the most robust (Figures 6 and S18). Changes in PEx/SDEx lie mostly toward or beyond the limits of uncertainty estimates (Figure S17), thus pointing toward non-stationarity in rainfall extremes. A power-type (Lomax) and a stretched-exponential (Weibull) tail have been used, with Lomax being a better fit over MtWest and Weibull over the rest of the domain.

An intensification complying with expectations based upon basic thermodynamic principles would possibly be expressed as a roughly uniform transfer of the tail toward greater rainfall values along a thermodynamic (~CC rate) trajectory (Figure 9a). In terms of tail properties, such a change would be translated to an increase in the scale parameter with

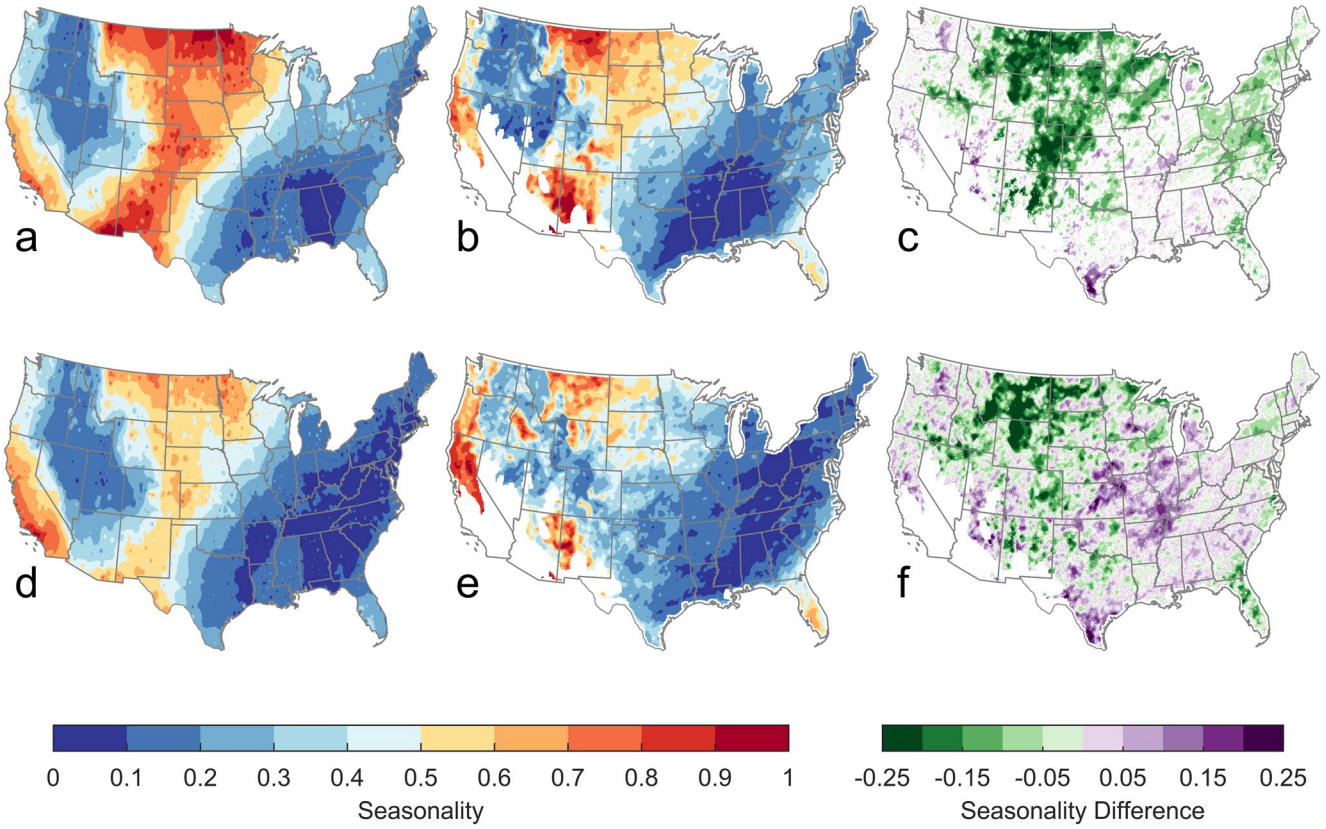

Figure 7. Tail seasonality: Maps of PEx seasonality indices based on (a) station data and (b) the CTL-WRF simulation. (c) Difference between the PGW-WRF and CTL-WRF seasonality index. Purple color indicates gridpoints where seasonality index increases in the future. Only gridpoints with statistically significant changes in seasonality are shown. (d–f) Same as (a–c), but for SDEx. PEx, Precipitation Extremes; PGW, Pseudo Global Warming; SDEx, Storm Depth Extremes; WRF, Weather Research and Forecasting model.

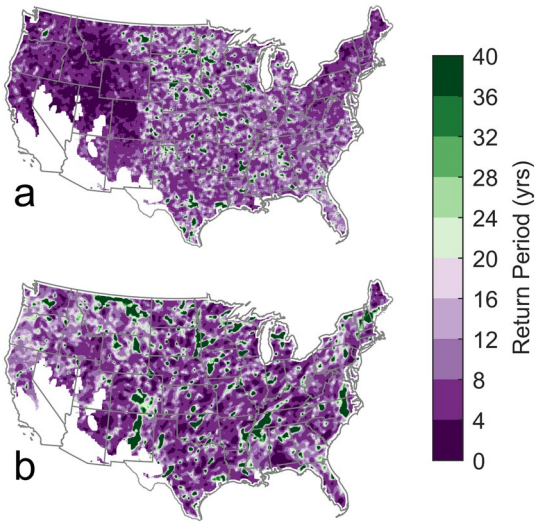

Figure 8. Changes in 20-year rainfall: Map of the return period estimated based on the PGW-WRF simulation, corresponding to the 20-years (a) PEx and (b) SDEx obtained by the CTL-WRF simulation. PEx, Precipitation Extremes; PGW, Pseudo Global Warming; WRF, Weather Research and Forecasting model.

a roughly unchanged tail index. However, our results show a dipole of different flavors of intensification, with strong scale parameter increases over the south/southeast and strong heaviness increases over the rest of the domain (Figure 9b). This dipole suggests that even though simple thermodynamics may serve as a common basis for PEx intensification, more complex mechanisms exacerbate this signal (Pfahl et al., 2017) and increases in heaviness are also exhibited.

Our results add to the wide scientific consensus toward rainfall intensification (Westra et al., 2014) and confirm previous findings that suggest an intensification throughout the US (Bador et al., 2018; Barbero et al., 2019; Cannon & Innocenti, 2019; Easterling et al., 2017; Fischer et al., 2013; Pfahl et al., 2017; Prein, Liu, Ikeda, Trier, et al., 2017; Prein, Rasmussen, et al., 2017). A similar decrease in PEx seasonality has only recently been demonstrated over Europe based on continental-wide CPM future projections (Chan et al., 2020). Examining the statistical properties of rainfall tails can support a more comprehensive understanding of PEx intensification compared to approaches based on commonly used extreme indices. Cannon et al. (Cannon & Innocenti, 2019) using the same dataset studied changes in intensity-duration-frequency curves and revealed that intensification is greater in finer than coarser temporal scales. The added value of CPMs toward this end has been already documented in recent studies (Ban et al., 2018; Kendon et al., 2017; Knist et al., 2020; Prein

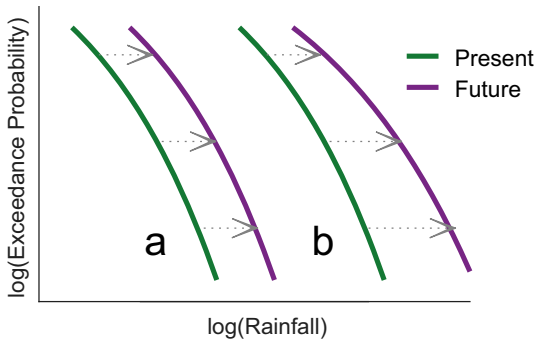

Figure 9. Schematic representation of different types of PEx intensification: (a) PEx intensification based on basic thermodynamic principles, exhibited with increases in scale parameter. (b) PEx intensification with increases in heaviness. PEx, Precipitation Extremes.

et al., 2015) and our analysis benefits from the increased WRF resolution (~4 km, 1 h) which allows to investigate PEx/SDEx changes at hydrologically relevant spatiotemporal scales. This can reveal the link between rainfall intensification, topography, atmospheric convection and the weather patterns affecting a region.

To reveal this physical link, PEx seasonality and PEx sensitivity to surface air temperature can prove to be very helpful. In fact, a remarkable similarity exists between the spatial pattern of tail heaviness (Figure 2b), PEx seasonality (Figure 3b) and the spatial pattern of PEx scaling with surface air and dewpoint temperature shown by Moustakis et al. (2020) (Figure S19). In general, higher (lower) scaling rates correspond to heavier (thinner) tails with a more (less) intense seasonal signal. Understanding this pivotal role of scaling rates as jointly reflecting non-linearity and seasonality is very important in order to properly interpret studies focusing on scaling estimations and assess their applicability in climate change studies. The shape parameter and the seasonality index used here are more direct measurements of non-linearity and seasonality respectively than scaling estimations. This is why seasonality and heaviness changes revealed here are only slightly reflected in changes in future scaling rates (Figure S19). In agreement with Prein, Rasmussen, et al. (2017) who presented spatially aggregated results, scaling rates remain relatively unchanged in a warmer climate, even though at a non-aggregated level increases appear over gridpoints with strong increases in heaviness.

Positive scaling rates (Moustakis et al., 2020) (Figure S19) suggest an increasing temperature gradient within the tail, meaning that the most extreme events occur at warmer temperatures. Indeed, the upper parts of rainfall tails tend to cluster more strongly within the warm months throughout the domain (Figure S6), except for the Pacific coast, where the most extreme PEx occur during winter (Figures S6 and S19).

In regions where heaviness increases, relative PEx changes are stronger for the higher percentiles, which, given the above, occur mostly at warmer temperatures. It is known that under higher temperatures vigorous atmospheric convection producing severe storms organized at the local or larger spatial scales occurs. As a result, increases in heaviness point toward changes in strong convection. Indeed, conditions are generally more favorable to severe convection and occur more frequently in PGW-WRF (Rasmussen et al., 2017). In particular more energy is available for convection to occur, as expressed by increases in Convective Available Potential Energy (CAPE) (Rasmussen et al., 2017). However, Convective Inhibition (CIN) also increases, meaning that more energy is necessary so that convection can actually occur. This simultaneous increase in CAPE and CIN means that weaker convective events are suppressed and become less frequent, but, when convection does occur, exceeding the increased CIN suppression, it can be significantly more vigorous (Rasmussen et al., 2017).

Increases in heaviness are revealed over MtWest (Figure 3), where the frequency of intense convection especially during July-August strongly increases (Rasmussen et al., 2017) and the most extreme PEx are mostly clustered within the warm months (Figure S6). Similarly, heaviness increases over the North Atlantic, the Plains and the Prairie, where strong convection becomes more frequent as well (Prein, Liu, Ikeda, Trier, et al., 2017; Rasmussen et al., 2017). These changes in heaviness over the regions where events of strong convective and non-convective nature coexist within the tails imply that events of strong convective nature get more severely intensified than non-convective ones. This appears to distort the expected uniform thermodynamic signal, leading to increases in heaviness (Figure 9b). Such a differential intensification between different storm types has been reported throughout the literature over the recent years (Berg & Haerter, 2013; Berg et al., 2013; Ivancic & Shaw, 2016; Lenderink et al., 2017; Molnar et al., 2015) and our results further support this finding.

Over the South, events of strong convective nature occurring throughout the year (Haberlie & Ashley, 2019; Z. Feng et al., 2019) probably already dominate PEx tails and, hence, increases in heaviness are not exhibited. In fact the expected severe increases in CAPE, CIN, and precipitable water (Rasmussen et al., 2017) are

reflected in the strong increases of scale parameters, especially during the warmer months over the South (Figure 3f).

Given the above, even though one would reasonably expect that more uniform changes, complying with thermodynamical expectations, would be exhibited over regions where non-convective events dominate the tail, this is not the case. In fact, over the Pacific Coast, heaviness also increases. This suggests that, although convective events have been the main focus of research recently (Prein, Liu, Ikeda, Bullock, et al., 2017; Prein, Liu, Ikeda, Trier, et al., 2017; Prein, Rasmussen, et al., 2017; Rasmussen et al., 2017; Scaff et al., 2019), changes in non-convective storms seem to be intensifying beyond simplistic thermodynamical expectations as well, especially if the changes in SDEx durations are also considered. The added value of CPMs in simulating the interplay of orography with larger-scale dynamics (Prein et al., 2015) can prove to be quite useful toward understanding the mechanisms driving such changes.

Even though strong convection which is by nature vigorous and of shorter duration is expected to dominate rainfall tails at the hourly scale, this is not necessarily the case when aggregating to larger temporal scales (Berg & Haerter, 2013; Berg et al., 2013; Ivancic & Shaw, 2016). Upon temporal aggregation, non-convective events generated by larger-scale disturbances (e.g. extra-tropical cyclones, frontals) might become more dominant within the tails, even in regions where severe convection occurs. In fact extra-tropical cyclones and frontals jointly constitute ~78% of daily rainfall extremes over the US (Kunkel et al., 2012). Hence, when SDEx are examined non-convective events become increasingly present within the tails throughout the domain and increases in heaviness are evident.

We suggest that such a physical conceptualization of rainfall intensification that links changes in the tail's statistical properties with storm types affecting a region could help modelers to constrain parameter changes in non-stationary simulations (Papalexiou, Markonis, et al., 2018).

Rainfall extremes greatly shape multiple earth system processes, from the hydrological response of river basins to more complex ecosystem dynamics and the intensification revealed here is expected to affect all those processes (Paschalis et al., 2015, 2020). It is expected that xeric and hydric ecosystems could benefit from more intense and less frequent rainfall events (Knapp et al., 2008), while productivity could be reduced over mesic ecosystems (Felton et al., 2020; Knapp et al., 2008). This is particularly relevant for grasslands which are highly sensitive to rainfall variability (Felton et al., 2020). Such ecosystems are common over the US and serve as livestock grazing lands that are significant for local food access and economies (Sloat et al., 2018). An increased water stress related to changes in PEx/SDEx could also affect rainfed crop yields over those regions, which are known to be more sensitive to climatic extremes than irrigated ones (Troy et al., 2015). In fact our results show that not only do PEx/SDEx intensify over the grasslands and crops of the Prairie and the Plains, but also that those regions constitute hotspots of changes in seasonality and storm duration (Figures 7 and 6). Impacts in crop and grassland yields due to these changes can have major consequences, which will will only be added to the significant impacts on ecosystems related to rising temperature and elevated CO2 levels alone (Fatichi, Leuzinger, et al., 2016; Mastrotheodoros et al., 2020; Paschalis et al., 2018).

Changes in ecosystem responses are expected to further alter convective activity, through land-atmosphere feedbacks (Bonetti et al., 2015; Manoli et al., 2016; Yin et al., 2015). Along with the free atmospheric state and atmospheric stability, soil water content, which is strongly coupled with vegetation dynamics codetermines the partitioning of radiation to latent and sensible heat fluxes, and hence, the expansion and water content of the atmospheric boundary layer as well (Bonetti et al., 2015; Manoli et al., 2016; Yin et al., 2015). As a result, not only is ecosystem functioning altered by increased convective activity, but at the same time, vegetation dynamics strongly influence convective rainfall predisposition as well. Such feedbacks could be related with rainfall intensification over semi-arid regions revealed in this study, which are known hotspots of strong land-atmosphere coupling (Koster et al., 2006).

Here we suggest that rainfall intensification might be experienced in ways beyond basic thermodynamic expectations. Changes in seasonality indicate PEx/SDEx occurring under different vegetation growth states and soil moisture regimes than previously experienced. Decreases in storm duration suggest a more limited capacity of vegetation and soil to intercept and absorb water, suggesting increased flood volumes. Changes in the spatial structure of storms could be expected as well and could further alter catchment flood responses (Chen et al., 2020; Peleg et al., 2019; Prein, Liu, Ikeda, Trier, et al., 2017).

WRF is able to reproduce the spatial characteristics of rainfall tails compared to station data. When direct comparisons are made, an underestimating bias is evident, as documented in more detail in Figure S20. A distinct bias over MtWest is revealed (Moustakis et al., 2020), however the station network over this region is extremely sparse with most stations being located within valleys and near populated areas. As a result, we cannot have much confidence about the true spatial characteristics of rainfall tails over this mountainous region and model validation at such fine spatiotemporal scales is uncertain. An overestimating bias in heaviness has also been exhibited over the rest of the domain, except for the Pacific Coast, while biases in simulating seasonality and SDEx duration are also documented. Model deviations could partly be attributed to the uncertainty related to the small sample sizes (13-years simulations). Despite that, our study focuses on WRF's ability to represent the spatial pattern in qualitative terms mostly. A more in depth model evaluation is beyond its scope and has already been performed (Dai et al., 2017; Cannon & Innocenti, 2019; Liu et al., 2017; Prein, Liu, Ikeda, Bullock, et al., 2017; Prein, Liu, Ikeda, Trier, et al., 2017; Prein, Rasmussen, et al., 2017; Rasmussen et al., 2017; Scaff et al., 2019).

It should be noted that under the PGW approach the large-scale dynamic forcing (ERA-Interim) remains the same and the climate forcing is only perturbed according to CMIP5 projections. As a result, possible changes in larger-scale dynamics and their associated mechanisms that may be experienced under climate change are by definition not accounted for. In reality, significant changes in larger-scale dynamics might exacerbate or even mask this signal. However, under CMIP5, larger-scale dynamics are not so prominent over the US (Liu et al., 2017) and, hence, the use of the PGW approach is justified.

Model resolution and deficiencies in simulating rainfall and other complex physical processes related to precipitation formation limit all climate change studies and further improvement is still needed (Prein et al., 2015). However, continental-wide CPM outputs are currently the best tool at hand for such purposes. Of course, it remains uncertain whether the rainfall intensification revealed here will be experienced in real-world. However, our results can definitely provide insight for real-world changes, to the extent that they are examined for what they are; representations of the changes in the models' reality. In that regard, the nature of intensification revealed here can be highly relevant for real-world climate, as long as interpretations are made with caution and model biases are taken into consideration.

Sample size can also be limiting and longer simulations with multiple ensemble members, accounting for internal variability are needed in order to further solidify our confidence over the results. Given the computational resources that are becoming increasingly available (Prein et al., 2015) it might be possible that multi-ensemble, multi-year continental-wide or even global simulations with CPMs could be performed in the near future.

Conflict of Interest

The authors declare no competing interests.

Data Availability Statement

All observational data are freely available and obtained by National Oceanic and Atmospheric Administration (NOAA), HPD: https://data.nodc.noaa.gov/cgi-bin/iso?id=gov.noaa.ncdc:C00127 and ISD: https://www.ncdc.noaa.gov/isddatabases sites. The High Resolution Weather Research and Forecasting (WRF) Simulations of the Current and Future Climate of North America is obtained by the Research Data Archive (RDA) of the National Center for Atmospheric Research (NCAR) (https://rda.ucar.edu/datasets/ds612.0/). All required code and rasters are publicly available in a Zenodo repository.

Acknowledgments
Y. Moustakis acknowledges funding from the Skempton Fellowship, of the Department of Civil and Environmental Engineering, Imperial College London. A. Paschalis acknowledges funding from NERC (NE/S003495/1).

References

Ali, H., Modi, P., & Mishra, V. (2019). Increased flood risk in Indian sub-continent under the warming climate. *Weather and Climate Extremes*, *25*, 100212. https://doi.org/10.1016/j.wace.2019.100212

Bador, M., Donat, M. G., Geoffroy, O., & Alexander, L. V. (2018). Assessing the robustness of future extreme precipitation intensification in the CMIP5 ensemble. *Journal of Climate*, *31*(16), 6505–6525. https://doi.org/10.1175/JCLI-D-17-0683.1

Ban, N., Rajczak, J., Schmidli, J., & Schär, C. (2018). Analysis of Alpine precipitation extremes using generalized extreme value theory in convection-resolving climate simulations. *Climate Dynamics*, *55*(61-75), 1–15. https://doi.org/10.1007/s00382-018-4339-4

Barbero, R., Fowler, H. J., Blenkinsop, S., Westra, S., Moron, V., Lewis, E., et al. (2019). A synthesis of hourly and daily precipitation extremes in different climatic regions. *Weather and Climate Extremes*, *26*, 100219. https://doi.org/10.1016/j.wace.2019.100219

Berg, P., & Haerter, J. O. (2013). Unexpected increase in precipitation intensity with temperature—A result of mixing of precipitation types? *Atmospheric Research*, *119*, 56–61. https://doi.org/10.1016/j.atmosres.2011.05.012

Berg, P., Moseley, C., & Haerter, J. O. (2013). Strong increase in convective precipitation in response to higher temperatures. *Nature Geoscience*, *6*(3), 181–185. https://doi.org/10.1038/ngeo1731

Berthou, S., Kendon, E. J., Chan, S. C., Ban, N., Leutwyler, D., Schär, C., & Fosser, G. (2018). Pan-European climate at convection-permitting scale: a model intercomparison study. *Climate Dynamics*, *55*(1), 35–59. https://doi.org/10.1007/s00382-018-4114-6

Bonetti, S., Manoli, G., Domec, J.-C., Putti, M., Marani, M., & Katul, G. G. (2015). The influence of water table depth and the free atmospheric state on convective rainfall predisposition. *Water Resources Research*, *51*(4), 2283–2297. https://doi.org/10.1002/2014WR016431

Bukovsky, M. (2011). *Masks for the Bukovsky regionalization of north America*. Regional Integrated Sciences Collective, Institute for Mathematics Applied to Geosciences, National Center for Atmospheric Research. Retrieved from http://www.narccap.ucar.edu/contrib/bukovsky/

Byrne, M. P., Pendergrass, A. G., Rapp, A. D., & Wodzicki, K. R. (2018). Response of the intertropical convergence zone to climate change: location, width, and strength. *Current Climate Change Reports*, *4*(4), 355–370. https://doi.org/10.1007/s40641-018-0110-5

Cannon, A. J., & Innocenti, S. (2019). Projected intensification of sub-daily and daily rainfall extremes in convection-permitting climate model simulations over North America: Implications for future intensity-duration-frequency curves. *Natural Hazards and Earth System Sciences*, *19*(2), 421–440. https://doi.org/10.5194/nhess-19-421-2019

Chan, S. C., Kendon, E. J., Berthou, S., Fosser, G., Lewis, E., & Fowler, H. J. (2020). Europe-wide precipitation projections at convection permitting scale with the unified model. *Climate Dynamics*, *55*(3), 409–428. https://doi.org/10.1007/s00382-020-05192-8

Chen, Y., Paschalis, A., Kendon, E., kim, D., & Onof, C. (2020). Changing spatial structure of summer heavy rainfall, using convection-permitting ensemble. *Geophysical Research Letters*, *48*(3), e2020GL090903. https://doi.org/10.1029/2020GL090903

Cover, T., & Joy, T. (2005). *Elements of information theory*. John Wiley & Sons, Ltd. Retrieved from https://onlinelibrary.wiley.com/doi/abs/10.1002/047174882X.ch2

Cutter, S. L., Barnes, L., Berry, M., Burton, C., Evans, E., Tate, E., & Webb, J. (2008). A place-based model for understanding community resilience to natural disasters. *Global Environmental Change*, *18*(4), 598–606. https://doi.org/10.1016/j.gloenvcha.2008.07.013

Dai, A., Rasmussen, R. M., Liu, C., Ikeda, K., & Prein, A. F. (2017). A new mechanism for warm-season precipitation response to global warming based on convection-permitting simulations. *Climate Dynamics*, *55*, 343–368. https://doi.org/10.1007/s00382-017-3787-6

Easterling, D. R., Kunkel, K., Arnold, J., Knutson, T., LeGrande, A., Leung, L. R., et al. (2017). Precipitation change in the United States. In *Climate Science Special Report: A Sustained Assessment Activity of the U.S. Global Change Research Program*. (pp. 301–335). U.S. Department of Commerce. https://digitalcommons.unl.edu/usdeptcommercepub/586/

Fatichi, S., Ivanov, V. Y., Paschalis, A., Peleg, N., Molnar, P., Rimkus, S., et al. (2016). Uncertainty partition challenges the predictability of vital details of climate change. *Earth's Future*, *4*(5), 240–251. https://doi.org/10.1002/2015EF000336

Fatichi, S., Leuzinger, S., Paschalis, A., Langley, J. A., Donnellan Barraclough, A., & Hovenden, M. J. (2016). Partitioning direct and indirect effects reveals the response of water-limited ecosystems to elevated CO_2. *Proceedings of the National Academy of Sciences*, *113*(45), 12757–12762. https://doi.org/10.1073/pnas.1605036113

Felton, A. J., Slette, I. J., Smith, M. D., & Knapp, A. K. (2020). Precipitation amount and event size interact to reduce ecosystem functioning during dry years in a mesic grassland. *Global Change Biology*, *26*(2), 658–668. https://doi.org/10.1111/gcb.14789

Feng, X., Porporato, A., & Rodriguez-Iturbe, I. (2013). Changes in rainfall seasonality in the tropics. *Nature Climate Change*, *3*(9), 811–815. https://doi.org/10.1038/nclimate1907

Feng, Z., Houze, R. A., Leung, L. R., Song, F., Hardin, J. C., Wang, J., et al. (2019). Spatiotemporal characteristics and large-scale environments of mesoscale convective systems east of the Rocky Mountains. *Journal of Climate*, *32*(21), 7303–7328. https://doi.org/10.1175/JCLI-D-19-0137.1

Fischer, E. M., Beyerle, U., & Knutti, R. (2013). Robust spatially aggregated projections of climate extremes. *Nature Climate Change*, *3*(12), 1033–1038. https://doi.org/10.1038/nclimate2051

Fischer, E. M., & Knutti, R. (2014). Detection of spatially aggregated changes in temperature and precipitation extremes. *Geophysical Research Letters*, *41*(2), 547–554. https://doi.org/10.1002/2013GL058499

Fischer, E. M., & Knutti, R. (2016). Observed heavy precipitation increase confirms theory and early models. *Nature Climate Change*, *6*(11), 986–991. https://doi.org/10.1038/nclimate3110

Fischer, E. M., Sedláček, J., Hawkins, E., & Knutti, R. (2014). Models agree on forced response pattern of precipitation and temperature extremes. *Geophysical Research Letters*, *41*(23), 8554–8562. https://doi.org/10.1002/2014GL062018

Guerreiro, S. B., Fowler, H. J., Barbero, R., Westra, S., Lenderink, G., Blenkinsop, S., et al. (2018). Detection of continental-scale intensification of hourly rainfall extremes. *Nature Climate Change*, *8*(9), 803–807. https://doi.org/10.1038/s41558-018-0245-3

Haberlie, A. M., & Ashley, W. S. (2019). A radar-based climatology of mesoscale convective systems in the United States. *Journal of Climate*, *32*(5), 1591–1606. https://doi.org/10.1175/JCLI-D-18-0559.1

Held, I. M., & Soden, B. J. (2006). Robust responses of the hydrological cycle to global warming. *Journal of Climate*, *19*(21), 5686–5699. https://doi.org/10.1175/JCLI3990.1

Hoerling, M., Eischeid, J., Perlwitz, J., Quan, X.-W., Wolter, K., & Cheng, L. (2016). Characterizing recent trends in US heavy precipitation. *Journal of Climate*, *29*(7), 2313–2332. https://doi.org/10.1175/JCLI-D-15-0441.1

Ivancic, T. J., & Shaw, S. B. (2016). A U.S.-based analysis of the ability of the Clausius-Clapeyron relationship to explain changes in extreme rainfall with changing temperature. *Journal of Geophysical Research*, *121*(7), 3066–3078. https://doi.org/10.1002/2015JD024288

Kendon, E. J., Ban, N., Roberts, N. M., Fowler, H. J., Roberts, M. J., Chan, S. C., et al. (2017). Do convection-permitting regional climate models improve projections of future precipitation change? *Bulletin of the American Meteorological Society*, *98*(1), 79–93. https://doi.org/10.1175/BAMS-D-15-0004.1

Knapp, A. K., Beier, C., Briske, D. D., Classen, A. T., Luo, Y., Reichstein, M., et al. (2008). Consequences of more extreme precipitation regimes for terrestrialEcosystems. *BioScience*, *58*(9), 811–821. https://doi.org/10.1641/B580908

Knist, S., Goergen, K., & Simmer, C. (2020). Evaluation and projected changes of precipitation statistics in convection-permitting WRF climate simulations over Central Europe. *Climate Dynamics*, *55*(1), 325–341. https://doi.org/10.1007/s00382-018-4147-x

Koster, R. D., Sud, Y. C., Guo, Z., Dirmeyer, P. A., Bonan, G., Oleson, K. W., et al. (2006). GLACE: The global land-atmosphere coupling experiment. Part I: Overview. *Journal of Hydrometeorology*, *7*(4), 590–610. https://doi.org/10.1175/JHM510.1

Kunkel, K. E., Easterling, D. R., Kristovich, D. A. R., Gleason, B., Stoecker, L., & Smith, R. (2012). Meteorological causes of the secular variations in observed extreme precipitation events for the conterminous United States. *Journal of Hydrometeorology*, *13*(3), 1131–1141. https://doi.org/10.1175/JHM-D-11-0108.1

Lenderink, G., Barbero, R., Loriaux, J. M., & Fowler, H. J. (2017). Super-Clausius-Clapeyron scaling of extreme hourly convective precipitation and its relation to large-scale atmospheric conditions. *Journal of Climate*, *30*(15), 6037–6052. https://doi.org/10.1175/JCLI-D-16-0808.1

Lenderink, G., & Van Meijgaard, E. (2008). Increase in hourly precipitation extremes beyond expectations from temperature changes. *Nature Geoscience*, *1*(8), 511–514. https://doi.org/10.1038/ngeo262

Liu, C., Ikeda, K., Rasmussen, R., Barlage, M., Newman, A. J., Prein, A. F., et al. (2017). Continental-scale convection-permitting modeling of the current and future climate of North America. *Climate Dynamics*, *49*(1–2), 71–95. https://doi.org/10.1007/s00382-016-3327-9

Manoli, G., Domec, J.-C., Novick, K., Oishi, A. C., Noormets, A., Marani, M., & Katul, G. (2016). Soil-plant-atmosphere conditions regulating convective cloud formation above southeastern US pine plantations. *Global Change Biology*, *22*(6), 2238–2254. https://doi.org/10.1111/gcb.13221

Markonis, Y., Papalexiou, S. M., Martinkova, M., & Hanel, M. (2019). Assessment of water cycle intensification over land using a multisource global gridded precipitation dataSet. *Journal of Geophysical Research: Atmospheres*, *124*(21), 11175–11187. https://doi.org/10.1029/2019JD030855

Mastrotheodoros, T., Pappas, C., Molnar, P., Burlando, P., Manoli, G., Parajka, J., et al. (2020). More green and less blue water in the Alps during warmer summers. *Nature Climate Change*, *10*(2), 155–161. https://doi.org/10.1038/s41558-019-0676-5

Molnar, P., Fatichi, S., Gaál, L., Szolgay, J., & Burlando, P. (2015). Storm type effects on super Clausius-Clapeyron scaling of intense rainstorm properties with air temperature. *Hydrology and Earth System Sciences*, *19*(4), 1753–1766. https://doi.org/10.5194/hess-19-1753-2015

Moustakis, Y., Onof, C. J., & Paschalis, A. (2020). Atmospheric convection, dynamics and topography shape the scaling pattern of hourly rainfall extremes with temperature globally. *Communications Earth & Environment*, *1*(1), 11. https://doi.org/10.1038/s43247-020-0003-0

O'Gorman, P. A. (2015). Precipitation Extremes Under Climate Change. *Current Climate Change Reports*, *1*(2), 49–59. https://doi.org/10.1007/s40641-015-0009-3

O'Gorman, P. A., & Schneider, T. (2009). The physical basis for increases in precipitation extremes in simulations of 21st-century climate change. *Proceedings of the National Academy of Sciences*, *106*(35), 14773–14777. https://doi.org/10.1073/pnas.0907610106

Papalexiou, S. M., AghaKouchak, A., & Foufoula-Georgiou, E. (2018). A diagnostic framework for understanding climatology of tails of hourly precipitation extremes in the United States. *Water Resources Research*, *54*(9), 6725–6738. https://doi.org/10.1029/2018WR022732

Papalexiou, S. M., Markonis, Y., Lombardo, F., AghaKouchak, A., & Foufoula-Georgiou, E. (2018). Precise temporal disaggregation preserving marginals and correlations (dipmac) for stationary and nonstationary processes. *Water Resources Research*, *54*(10), 7435–7458. https://doi.org/10.1029/2018WR022726

Papalexiou, S. M., & Montanari, A. (2019). Global and Regional increase of precipitation extremes under global warming, *Water Resources Research*, *55*, 4901–4914. https://doi.org/10.1029/2018WR024067

Paschalis, A., Fatichi, S., Katul, G. G., & Ivanov, V. Y. (2015). Cross-scale impact of climate temporal variability on ecosystem water and carbon fluxes. *Journal of Geophysical Research: Biogeosciences*, *120*(9), 1716–1740. https://doi.org/10.1002/2015JG003002

Paschalis, A., Fatichi, S., Molnar, P., Rimkus, S., & Burlando, P. (2014). On the effects of small scale space-time variability of rainfall on basin flood response. *Journal of Hydrology*, *514*, 313–327. https://doi.org/10.1016/j.jhydrol.2014.04.014

Paschalis, A., Fatichi, S., Pappas, C., & Or, D. (2018). Covariation of vegetation and climate constrains present and future T/ET variability. *Environmental Research Letters*, *13*(10), 104012. https://doi.org/10.1088/1748-9326/aae267

Paschalis, A., Fatichi, S., Zscheischler, J., Ciais, P., Bahn, M., Boysen, L., et al. (2020). Rainfall-manipulation experiments as simulated by terrestrial biosphere models: Where do we stand? *Global Change Biology*, *26*(6), 3336–3355. https://doi.org/10.1111/gcb.15024

Peleg, N., Skinner, C., Fatichi, S., & Molnar, P. (2019). Temperature effects on heavy rainfall modify catchment hydro-morphological response. *Earth Surface Dynamics Discussions*, *8*, 17–36.Retrieved from https://www.earth-surf-dynam-discuss.net/esurf-2019-44/. https://doi.org/10.5194/esurf-2019-44

Pendergrass, A. G., & Hartmann, D. L. (2014). Changes in the distribution of rain frequency and intensity in response to global warming. *Journal of Climate*, *27*(22), 8372–8383. https://doi.org/10.1175/JCLI-D-14-00183.1

Pfahl, S., O'Gorman, P. A., & Fischer, E. M. (2017). Understanding the regional pattern of projected future changes in extreme precipitation. *Nature Climate Change*, *7*(6), 423–427. https://doi.org/10.1038/nclimate3287

Prein, A. F., Langhans, W., Fosser, G., Ferrone, A., Ban, N., Goergen, K., et al. (2015). A review on regional convection-permitting climate modeling: Demonstrations, prospects, and challenges. *Reviews of Geophysics*, *53*(2), 323–361. https://doi.org/10.1002/2014RG000475

Prein, A. F., Liu, C., Ikeda, K., Bullock, R., Rasmussen, R. M., Holland, G. J., & Clark, M. (2017). Simulating North American mesoscale convective systems with a convection-permitting climate model. *Climate Dynamics*, *55*(95-110), 1–16. https://doi.org/10.1007/s00382-017-3993-2

Prein, A. F., Liu, C., Ikeda, K., Trier, S. B., Rasmussen, R. M., Holland, G. J., & Clark, M. P. (2017). Increased rainfall volume from future convective storms in the US. *Nature Climate Change*, *7*(12), 880–884. https://doi.org/10.1038/s41558-017-0007-7

Prein, A. F., Rasmussen, R. M., Ikeda, K., Liu, C., Clark, M. P., & Holland, G. J. (2017). The future intensification of hourly precipitation extremes. *Nature Climate Change*, *7*(1), 48–52. https://doi.org/10.1038/nclimate3168

Rasmussen, K. L., Prein, A. F., Rasmussen, R. M., Ikeda, K., & Liu, C. (2017). Changes in the convective population and thermodynamic environments in convection-permitting regional climate simulations over the United States. *Climate Dynamics*, *55*, 383–408. https://doi.org/10.1007/s00382-017-4000-7

Scaff, L., Prein, A. F., Li, Y., Liu, C., Rasmussen, R., & Ikeda, K. (2019). Simulating the convective precipitation diurnal cycle in North America's current and future climate. *Climate Dynamics*, *55*(369-382), 1–14. https://doi.org/10.1007/s00382-019-04754-9

Sharma, A., Wasko, C., & Lettenmaier, D. P. (2018). If precipitation extremes are increasing, why aren't floods? *Water Resources Research*, *54*(11), 8545–8551. https://doi.org/10.1029/2018WR023749

Sloat, L. L., Gerber, J. S., Samberg, L. H., Smith, W. K., Herrero, M., Ferreira, L. G., et al. (2018). Increasing importance of precipitation variability on global livestock grazing lands. *Nature Climate Change*, *8*(3), 214–218. https://doi.org/10.1038/s41558-018-0081-5

Stratton, R. A., Senior, C. A., Vosper, S. B., Folwell, S. S., Boutle, I. A., Earnshaw, P. D., et al. (2018). A pan-African convection-permitting regional climate simulation with the met office unified model: CP4-Africa. *Journal of Climate*, *31*(9), 3485–3508. https://doi.org/10.1175/JCLI-D-17-0503.1

Troy, T. J., Kipgen, C., & Pal, I. (2015). The impact of climate extremes and irrigation on US crop yields. *Environmental Research Letters*, *10*(5), 054013. https://doi.org/10.1088/1748-9326/10/5/054013

Westra, S., Fowler, H. J., Evans, J. P., Alexander, L. V., Berg, P., Johnson, F., et al. (2014). Future changes to the intensity and frequency of short-duration extreme rainfall. *Reviews of Geophysics*, *52*(3), 522–555. https://doi.org/10.1002/2014RG000464

Yin, J., Albertson, J. D., Rigby, J. R., & Porporato, A. (2015). Land and atmospheric controls on initiation and intensity of moist convection: CAPE dynamics and LCL crossings. *Water Resources Research*, *51*(10), 8476–8493. https://doi.org/10.1002/2015WR017286